



Article

Core-Shell Structured SiO₂@NiFe LDH Composite for Broadband Electromagnetic Wave Absorption

Zhilan Du ^{1,†}, Dashuang Wang ^{1,†}, Xinfang Zhang ¹, Zhiyu Yi ¹, Jihai Tang ², Pingan Yang ³ , Rui Cai ³,
Shuang Yi ¹, Jinsong Rao ¹ and Yuxin Zhang ^{1,*}

¹ College of Material Science and Engineering, Chongqing University, Chongqing 400044, China

² No. 59 Research Institute of China Ordnance Industries, Chongqing 400039, China

³ School of Automation, Chongqing University of Posts and Telecommunications, Chongqing 400065, China

* Correspondence: zhangyuxin@cqu.edu.cn

† These authors contributed equally to this work.

Abstract: In this work, a novel core-shell structure material, NiFe layered double hydroxide (NiFe LDH) loaded on SiO₂ microspheres (SiO₂@NiFe LDH), was synthesized by a one-step hydrothermal method, and the spontaneous electrostatic self-assembly process. The morphology, structure, and microwave absorption properties of SiO₂@NiFe LDH nanocomposites with different NiFe element ratios were systematically investigated. The results show that the sample of SiO₂@NiFe LDH-3 nanocomposite has excellent microwave absorption properties. It exhibits broadband effective absorption bandwidth (RL < −10 dB) of 8.24 GHz (from 9.76 GHz to 18.0 GHz) and the reflection loss is −53.78 dB at the matched thickness of 6.95 mm. It is expected that this SiO₂@NiFe-LDH core-shell structural material can be used as a promising non-precious, metal-based material microwave absorber to eliminate electromagnetic wave contamination.

Keywords: SiO₂ microspheres; LDH; microwave absorption; core-shell structure



Citation: Du, Z.; Wang, D.; Zhang, X.; Yi, Z.; Tang, J.; Yang, P.; Cai, R.; Yi, S.; Rao, J.; Zhang, Y. Core-Shell Structured SiO₂@NiFe LDH Composite for Broadband Electromagnetic Wave Absorption. *Int. J. Mol. Sci.* **2023**, *24*, 504. <https://doi.org/10.3390/ijms24010504>

Academic Editor: Abderrazzak Douhal

Received: 29 November 2022

Revised: 17 December 2022

Accepted: 22 December 2022

Published: 28 December 2022



Copyright: © 2022 by the authors. Licensee MDPI, Basel, Switzerland. This article is an open access article distributed under the terms and conditions of the Creative Commons Attribution (CC BY) license (<https://creativecommons.org/licenses/by/4.0/>).

1. Introduction

In recent decades, with the wide application of electronic equipment in military, medical, life, and other scenarios, as well as the rapid development of 5G technology, electromagnetic interference and electromagnetic radiation problems have become increasingly serious, thereby presenting an urgent demand for electromagnetic absorption (EMA) materials [1–4]. It is well known that high-performance microwave absorbers working in the S, C, and X bands have achieved certain research progress [5]. As a promising absorber, SiO₂ not only has the advantages of low density, high stability, good dispersion, and structure, but also has excellent biocompatibility and can be combined with one-dimensional nanowires [6], two-dimensional nanosheets [7–9], effectively combining related novel structures [10–12]. In recent years, researchers believe that designing materials with core-shell structures are expected to make them effective microwave-absorbing materials. Wang et al. successfully prepared material graphene@SiO₂@NiO nanoflowers, which have good microwave absorption performance, and their RL_{min} value is −20.5 dB [13]. Qiao et al. constructed a novel egg yolk shell Fe₃O₄@void@SiO₂@PPy nanochains with a minimum RL value of −54.2 dB and an effective absorption bandwidth (RL < −10 dB) of 5.90 GHz [14]. Huang et al. successfully prepared a gradient FeNi-SiO₂ film to achieve a reflection loss of −55.2 dB at 2.5 mm [15]. These studies show that the microwave absorption performance of SiO₂ depends to a large extent on the structure and properties of its Supporting Materials [16]. Therefore, it is very meaningful to search for novel structural SiO₂-based core-shell materials with enhanced microwave attenuation properties.

Layered double hydroxides (LDHs) are known as 2D hydrotalcite-like materials and consist of a positively charged host layer and exchangeable interlayer anions with the general formula [M_{1-x}M_x²⁺M_x³⁺(−OH)₂(A^{n−})_{x/n}·mH₂O], where M²⁺ and M³⁺ represent

divalent and trivalent metals, and An- represent interlayer anion [17]. As the layered double hydroxides (LDHs) containing transition metal elements (Fe, Co, Ni, etc.) with high surface-to-volume ratio, controllable layered structure and tunable metal composition are expected to be excellent microwave absorbers [18]. LDH not only has a high specific surface area and a rich inner interface but also a stable point of structure, which provides favorable conditions for multiple reflections of incident electromagnetic waves after entering the material, thereby minimizing the attenuation of electromagnetic waves [19]. In addition, the relatively low conductivity of LDH can provide a good impedance match with the magnetic material composite so that more electromagnetic waves can easily enter the material, meeting the two advantages of high-quality absorbing materials. Therefore, LDH can be considered a promising electromagnetic wave absorbing material [20]. Moreover, compared with other LDHs, NiFe LDH is characterized by magnetic properties due to the presence of transition metals Ni and Fe, which can introduce a magnetic loss mechanism, and the magnetic-dielectric synergy can effectively match the characteristic impedance over a wide frequency range, thus broadening the effective absorption bandwidth [21]. Therefore, NiFe LDH is expected to be a promising material for electromagnetic wave absorption.

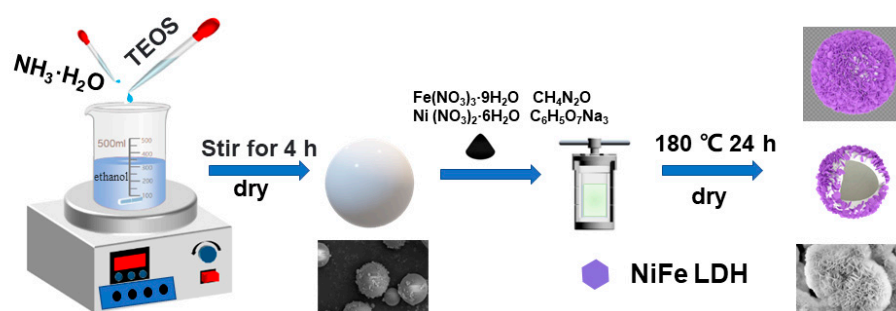
Currently, excellent electromagnetic wave absorption performance can be achieved by designing a core-shell structure of absorbers that combine dielectric loss and magnetic loss components. Well-designed core-shell nanosheets have a large specific surface area and abundant interfaces. With SiO₂ as the core, it is necessary to select a material with different loss mechanisms as the shell, meet the impedance matching conditions, and the different components work synergistically to improve the electromagnetic wave absorption performance [22]. Studies have shown that core-shell materials that satisfy both dielectric loss and magnetic loss have better performance and application prospects [23]. Magnetic loss, dielectric loss, dipole polarization, and superior impedance matching work together to obtain a microwave absorber with lightweight, thin thickness, wide frequency band, and strong absorption [24]. It has been found that low-dimensional, core-shell materials have considerable potential in improving the absorption performance of electromagnetic waves through their special structural properties and combined with the interface effect of the material itself, magnetic loss, dielectric loss, and impedance matching [25]. On this basis, magnetic LDH is very suitable as one of the candidate shell materials on SiO₂ due to its environmental stability, excellent magnetic permeability, and novel bilayer structure [26]. However, there are very few related reports so far. We can improve the impedance matching of SiO₂ materials by constructing LDH structures with different NiFe ratios, which endows a designable combination of spherical and layered structures, good matching of magnetic and electrical conductivity, and larger characteristic of the specific surface area, thereby enabling the material to obtain strong loss and broadband absorption properties at the same time [27]. By combining the excellent advantages of nano-SiO₂ and NiFe LDH, not only can the magnetic loss of NiFe LDH be fully utilized, but also the harmful electromagnetic waves can be further dissipated through the interface interaction between SiO₂ and NiFe LDH [28].

In this work, a one-step hydrothermal method was used to design and synthesize bimetallic hydroxide (NiFe-LDH) nanosheets grown on the surface of SiO₂ microspheres. Magnetic NiFe-LDH has a complex three-dimensional structure. By adjusting the ratio of Ni²⁺ and Fe³⁺ in NiFe LDH, good impedance matching, and high-performance microwave absorption can be obtained. The prepared SiO₂@NiFe LDH nanocomposites with different NiFe ratios have high impedance matching, the superior synergistic effect of dielectric loss and magnetic loss, and excellent microwave absorption performance. SiO₂@NiFe LDH nanocomposites have the characteristics of strong microwave scattering ability, light weight, strong absorption performance, and wide absorption bandwidth and are expected to become a new type of structural microwave absorption material.

2. Results

2.1. Structure Characterization and Analysis

The fabrication process of SiO₂@NiFe-LDH is displayed in Scheme 1. Firstly, the prepared SiO₂ microspheres were uniformly dispersed in an aqueous solution. A mixed solution containing nickel nitrate and ferric nitrate was added to the aqueous solution with urea as a precipitant. After the solution was mixed evenly by strong magnetic stirring, the solution was put into a rotary oven and heated at 180 °C for 24 h, and the brown precipitate was finally obtained. Under hydrothermal conditions, urea (CO(NH₂)₂) decomposes into ammonium ions (NH₄⁺), carbon dioxide (CO₂), and hydroxide ions (OH⁻). Then carbon dioxide (CO₂) is hydrolyzed into carbonate ions (CO₃²⁻) and hydrogen ions (H⁺). At the same time, metal cations (Ni²⁺ and Fe³⁺) combine with the hydroxide (OH⁻) to form layered double hydroxides on a silica substrate, while carbonate ions (CO₃²⁻) act as interlayer anions to maintain charge balance [29].



Scheme 1. The synthesis process of SiO₂@NiFe LDH composites.

To characterize and analyze the morphologies and lattice of the as-prepared samples on the nanoscale, SEM and TEM images were acquired, as shown in Figures S1 and S2, and Figure 1. The TEM images of Figure S2 and Figure 1a–c show that SiO₂@NiFe-LDH has a core-shell nanostructure, and the thickness of the LDH shell layer is less than 100 nm. As can be seen from the TEM images, the outer layer of SiO₂@NiFe-LDH-3 consists of a large number of nanosheets, which are superimposed together to form a large number of accumulation pores, forming a rich interface between each other. In Figure S3, when the molar ratio of Ni²⁺ and Fe³⁺ is 3:3, the nanosheets are thinner and grow vertically on the surface of SiO₂ spheres, which is conducive to improving the charge transfer efficiency. According to the HAADF mapping image in Figure 1e–i, there are Si, O, Ni, and Fe elements in SiO₂@NiFe LDH-3, SiO₂ microspheres provide Si and O elements, and LDH provides Ni, Fe, and O elements.

The XRD spectra of Figure S4 confirm the composition of pure SiO₂. Wide peaks in the XRD spectrum of SiO₂ indicate that it is an amorphous phase. Due to its inherent hydrophilicity, SiO₂ microspheres are conducive to the adsorption of Fe³⁺ and Ni²⁺ ions, promote the uniform coverage of Fe³⁺ and Ni²⁺ on the surface of SiO₂ microspheres, and grow in situ to form NiFe LDH nanosheets. In the XRD pattern (Figure 2a), the four diffraction peaks located at 2θ of 11.3°, 22.5°, 34.5°, and 59.7° correspond to (003), (006), (012) and (110) crystal planes, respectively, which are the characteristic diffraction peaks of LDH [30], further illustrating the successful in situ growth of a typical hydroxide-like material on the surface of SiO₂, wherein (003) the crystal plane spacing is 0.68 nm.

The hysteresis loop (M-H curve) of the SiO₂@NiFe LDH composites tested under 300 k conditions in the range of –15 Koe to 15 Koe is shown in Figure 2b. It can be seen that samples with three different molar ratios all exhibit typical weak ferromagnetic properties, that is, the magnetization intensity of the particles changes slightly with the increase of the applied magnetic field, and then reaches a saturation state. The saturation magnetization intensity Ms of SiO₂@NiFe LDH-1,2,3 was 0.75, 1.15, and 1.40 emu/g, respectively. As the molar ratio of Fe³⁺ increases, the coercivity of SiO₂@NiFe LDH composites also gradually increases. Among them, the S3 sample has the greatest coercive force (24.8 Oe).

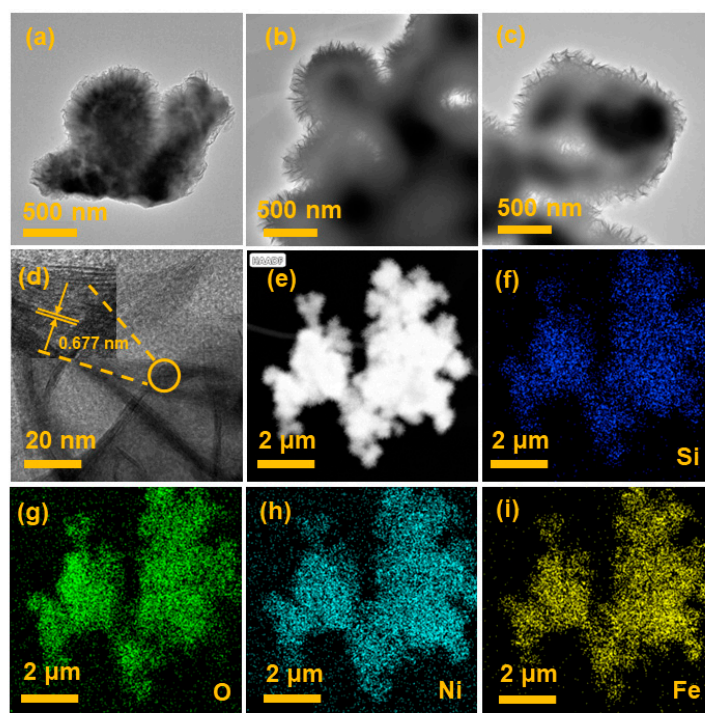


Figure 1. TEM images of (a) SiO₂@NiFe LDH-1, (b) SiO₂@NiFe LDH-2, (c,d) SiO₂@NiFe LDH-3, and (e–i) HAADF results for SiO₂@NiFe LDH-3.

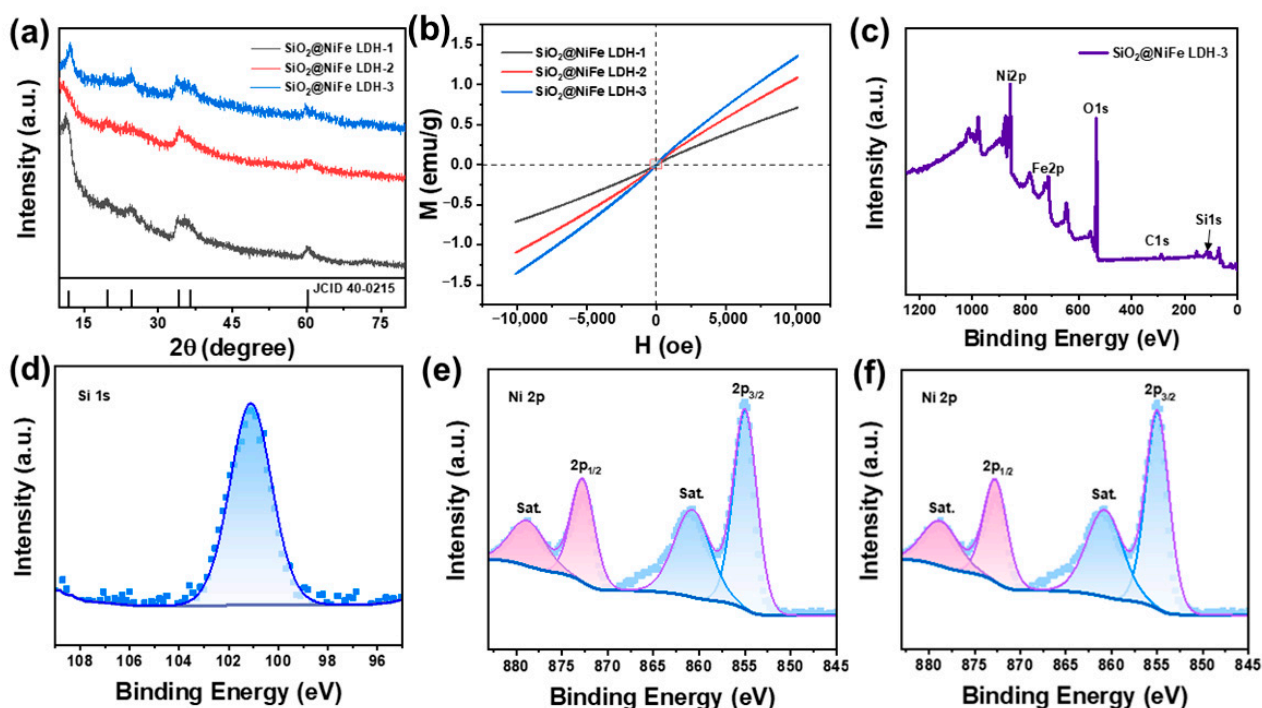


Figure 2. (a) XRD patterns, (b) magnetic hysteresis loops of SiO₂@NiFe LDH-1, 2, 3, and (c–f) XPS survey spectrum of SiO₂@NiFe LDH-3: (c) total spectra, (d) Si 2p, (e) Ni 2p, (f) Fe 2p.

XPS spectroscopy further verifies that the elements Ni, Fe, C, Si, and O in SiO₂@NiFe-LDH-3 (Figure 2c) conform to HAADF results. The combined energy of 856.5 eV and 874.1 eV is attributed to Ni 2p_{3/2} and Ni 2p_{1/2}, respectively, representing Ni²⁺ in SiO₂@NiFe-LDH microspheres. Signal sum at 713.3, 726.6 eV corresponds to Fe 2p_{3/2} and Fe 2p_{1/2}, implying Fe³⁺. XPS surveys of S3 (Figure 2b) showed that the six peaks were located at

857.23, 713.44, 533.7, 285.07, and 102.34 eV for Ni 2p, Fe 2p, O1s, C1s, and Si, where the corresponding atomic concentrations of Ni, Fe, O, C, and Si were 13.54%, 4.07%, 65.65%, 8.60%, and 8.14%, respectively.

FT-IR spectroscopy was performed on pure SiO₂ microspheres and SiO₂@NiFe LDH (Figure S5). The wide peak of pure SiO₂ near 1011.97 cm⁻¹ is due to the bending vibration of the physical absorption of water, and the weak adsorption peak at around 791 cm⁻¹ is due to the existence of the Si-O-Si bond. The characteristic peaks of -OH and physical adsorption water still exist at about 3384.77 cm⁻¹ and 1636.80 cm⁻¹ of SiO₂@NiFe LDH. The weak peak near 1007.78 cm⁻¹ is considered to be the intercalation structure of -OH and CO³⁻ in hydrotalcite (NiFe LDH). The bending vibration mode of metal hydroxide octahedral complexes (Ni-O and Fe-O) is observed at 594.97 cm⁻¹ and 663.99 cm⁻¹, respectively. The results show that NiFe LDH is formed on SiO₂ microspheres, which is consistent with the XRD characterization results. Thermal analysis (Figure S6a–c) shows that SiO₂@NiFe LDH-1, 2, 3 have two significant mass reduction processes during the temperature rise from 30 °C to 1000 °C. The weight loss of the S3 sample was 5.5635% at about 150 °C and 7.0129% at about 350 °C. This phenomenon is caused by the evaporation of adsorbed water and carbonate anion intercalation transition in NiFe LDH, respectively.

2.2. Electromagnetic Parameters and Microwave Absorption Properties

The composite material and paraffin were mixed evenly in a mass ratio of 4:6, and they were pressed into a circular sample using a mold with an inner diameter of 3.04 mm, an outer diameter of 7.00 mm, and a thickness of 2.00 mm. The composite permittivity ($\epsilon_r = \epsilon' - j\epsilon''$) and permeability ($\mu_r = \mu' - j\mu''$) were obtained by the coaxial method with a vector network analyzer in the frequency range 2–18 GHz. The electromagnetic wave absorption performance depends on electromagnetic parameters of materials [31]. This section systematically investigates the electromagnetic parameters of the absorbers of the prepared samples combined with paraffin.

Figure 3 shows the relative permittivity and relative permeability of the absorber. It can be seen from Figure 3a that the ϵ' constant decreases gradually, and the value is between 3 and 4, which is lower than the corresponding value of other NiFe-based materials reported in the literature [32,33]. For wave absorbing materials, an excessively high dielectric constant will generate an oscillating current on the surface of the material, and electromagnetic waves will be reflected instead of absorbed. On the contrary, a low dielectric constant is conducive to impedance matching, that is, it can allow more electromagnetic waves to be incident on the surface of the material. Among the materials, it has great benefits for the absorbing properties [34]. The gradually decreasing dielectric constant can be attributed to the typical dispersion response due to the increasing hysteresis of the dipole polarization response with respect to the electric field [35]. The relative permittivity of absorbing materials mainly depends on the space charge polarization and dipole polarization in the material, which have a strong dependence on frequency. It can be seen from Figure 3b that the imaginary part of the permittivity has obvious fluctuations in the high frequency part (14–18 GHz), which means that there is obvious polarization loss in the decay process of the incident electromagnetic wave and is due to the electron exchange between the Fe³⁺ and the Ni²⁺ in the NiFe-LDH inducing a large number of space charges and polarization charges under the action of the alternating electromagnetic field. Both polarizations increase the dielectric loss capability of the absorber, which is consistent with the frequency-dependence conclusion of our previous analysis [36]. Usually, the real part (ϵ' and μ') of the electromagnetic parameter represents the energy storage capacity of the absorbing material for electromagnetic energy, while the imaginary part (ϵ'' and μ'') represents the dissipation capacity of electrical and magnetic energy, respectively [37]. The real part and imaginary part of the dielectric constant of SiO₂@NiFe LDH-3 (S3) are the largest, which indicates that S3 has stronger electromagnetic storage ability and dielectric loss ability than the other two samples.

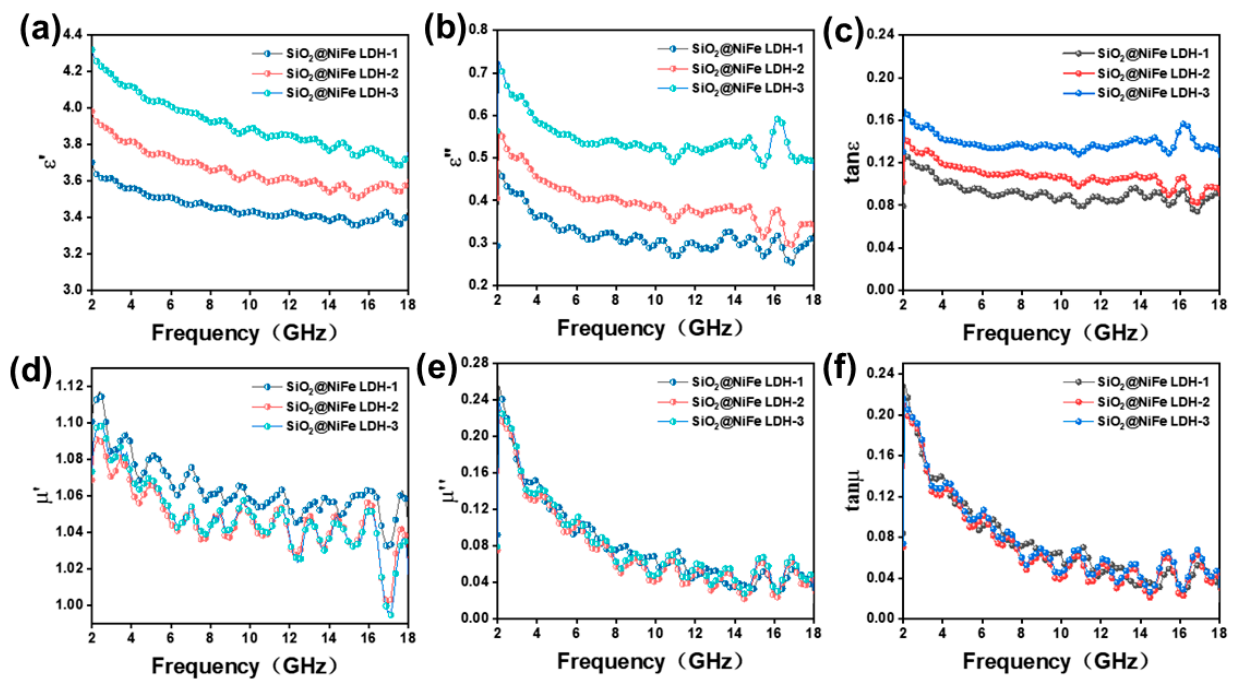


Figure 3. Frequency dependence of (a) the real and (b) the imaginary part of the complex dielectric constant, (d) the real part of the complex permeability and (e) the imaginary part, (c) $\tan \epsilon$ and (f) $\tan \mu$, of the three $\text{SiO}_2@NiFe$ LDH-1, 2, 3 with different Ni, Fe molar ratios.

Figure 3d,e show the variation curves of μ' and μ'' of $\text{SiO}_2@NiFe$ LDH with frequency. The three samples generally show a downward trend, and the fluctuation is more obvious. There are many factors that affect the μ' value, such as resonance, magnetic crystal anisotropy, exchange coupling effect and eddy current [38]. After the hydrothermal reaction, NiFe bimetallics form a layered bimetallic structure on SiO_2 microspheres, and with the increase of the relative content of Fe, which has strong magnetic properties, the saturation magnetization also corresponds. Enhancement (Figure 2b), the high M_s (1.5 emu/g), and low H_c (20 Oe) of the S3 samples help to improve the magnetic permeability and enhance the electromagnetic wave attenuation capability [39]. Therefore, the real part of the magnetic permeability of the S3 is relatively high. For the imaginary part curve, the three samples generally show a downward trend with obvious fluctuations. The trends of the three samples are very similar. Usually, the cause of magnetic loss is that the natural resonance behavior of the absorber causes large fluctuations in the low-frequency band, and the fluctuations in the high-frequency band are attributed to the switching resonance, which is part of the absorber's absorption mechanism [40].

The dielectric loss tangent and the magnetic loss tangent represent the dielectric loss capability and magnetic loss capability of the material, respectively. The higher the $\tan \delta_\epsilon$ or $\tan \delta_\mu$, the greater the ability of the sample to absorb electromagnetic waves through dielectric loss or magnetic loss [41]. The decreasing trend of $\tan \delta_\epsilon$ of the three samples in Figure 4c is almost the same, but there is a large fluctuation from 14 to 18 GHz, showing several obvious resonance peaks, which are similar to the resonance peaks of ϵ'' , indicating that there are multiple polarizations on the absorption surface relaxation, such as interfacial polarization and dipole polarization. The massive heterojunction between NiFe nanosheets on the microspheres and the SiO_2 matrix produces interfacial polarization, which weakens incident electromagnetic waves and leads to dielectric loss. In addition, the nano-sized NiFe nanosheet layered structure can act as a dipole, generate a large amount of orientation polarization, and convert electromagnetic wave energy into thermal energy, especially at low frequencies, indicating that S3 exhibits the best dielectric at low frequencies loss capacity. The difference in $\tan \delta_\mu$ values of the three samples in the figure is very small, and they all fluctuate between 0.02 and 0.24, indicating that the three samples have similar

magnetic loss capabilities. In addition, the $\tan \delta_\mu$ value of the three samples is greater than the $\tan \delta_\epsilon$ value at low frequencies; and the $\tan \delta_\epsilon$ is greater than the $\tan \delta_\mu$ value at high frequencies, indicating that the microwave absorption properties of the three samples originate from dielectric loss and magnetic loss and depend on the magnetic field at low frequencies. Loss depends on dielectric loss at high frequencies.

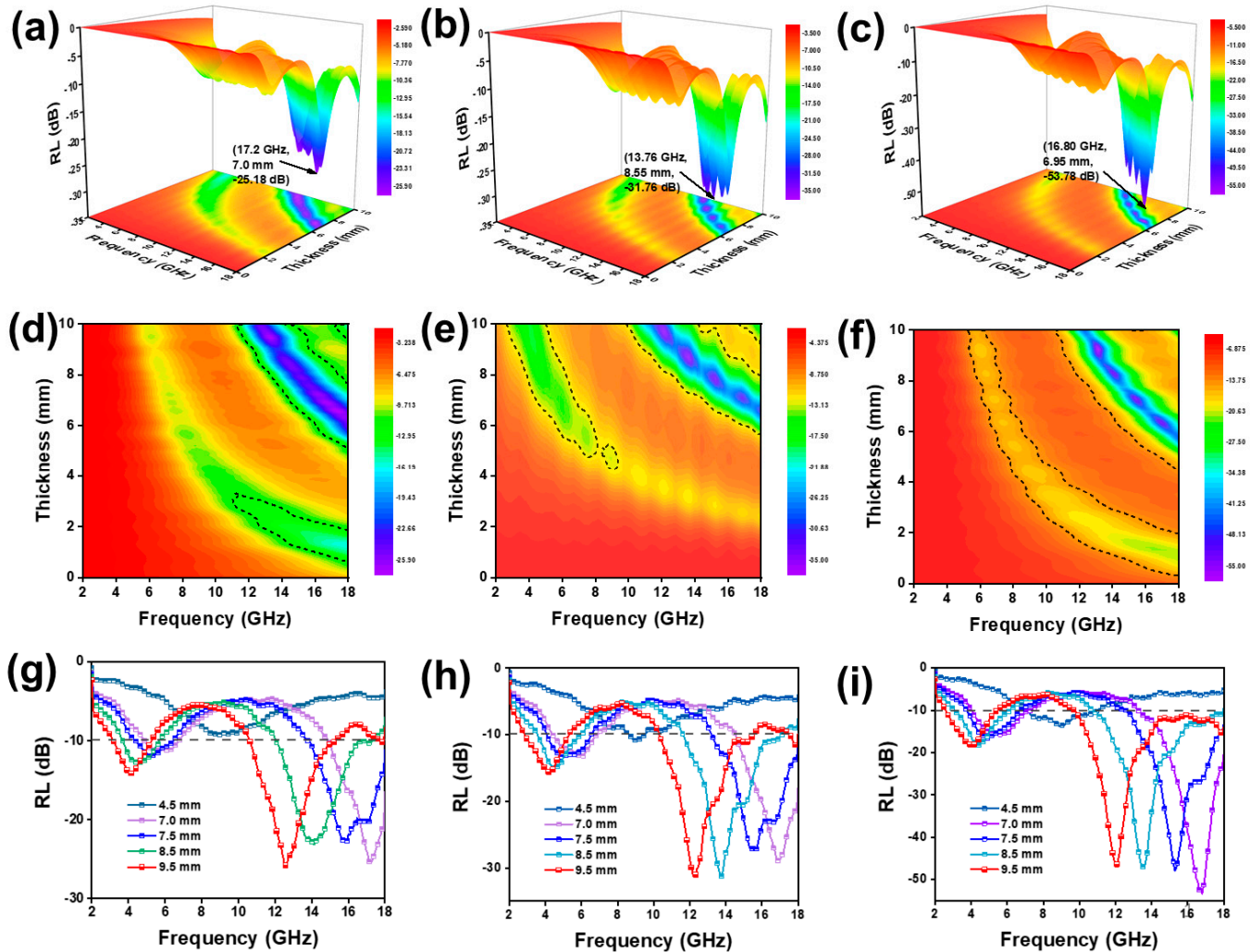


Figure 4. Corresponding 3D plots (a–c), 2D plots (d–f) with effective absorption bandwidth, and frequency dependence of RL values at different thickness: (g–i) SiO₂@NiFe LDH-1, SiO₂@NiFe LDH-2, SiO₂@NiFe LDH-3, respectively.

Debye relaxation is one of the important ways in which absorbing materials can produce dielectric losses. Usually Equation (3) can be derived from Equations (1) and (2), which can express the relationship between ϵ' and ϵ'' [42].

$$\epsilon' = \epsilon_\infty + \frac{\epsilon_s - \epsilon_\infty}{1 + \omega^2\tau^2} \tag{1}$$

$$\epsilon'' = \frac{\epsilon_s - \epsilon_\infty}{1 + \omega^2\tau^2}\omega\tau + \frac{\sigma}{\omega\epsilon_0} \tag{2}$$

Which could also be written as:

$$\left(\epsilon' - \frac{\epsilon_s - \epsilon_\infty}{2}\right)^2 + (\epsilon'')^2 = \left(\frac{\epsilon_s - \epsilon_\infty}{2}\right)^2 \tag{3}$$

where ϵ_s and ϵ_∞ are the static permittivity, optical permittivity, vacuum permittivity and angular frequency, respectively. Therefore, each semicircular curve represents a relaxation process. The SiO₂@NiFe LDHs exhibit obvious multiple Cole–Cole semicircles in Figure S7, but the semicircles have some disorder, which indicates strong multipole relaxation and decay, thereby confirming that SiO₂@NiFe LDH may be a mixed polarization model with interfacial polarization, electric dipole polarization, etc.

The reflection loss value (RL) of the absorber at 2–18 GHz corresponding to different thickness frequencies is calculated using the transmission line theory [43].

$$RL(dB) = 20 \log |(Z_{in} - Z_0) / (Z_{in} + Z_0)| \quad (4)$$

$$Z_{in} = Z_0 \sqrt{\mu_r / \epsilon_r} \tanh [j(2\pi f d / c) \sqrt{\mu_r \epsilon_r}] \quad (5)$$

where c , f , and d are the speed of light, the corresponding frequency, and the matching thickness, respectively. Z_{in} is the normalized input impedance; Z_0 is the free space impedance; and ϵ_r and μ_r are the complex permittivity and complex permeability, respectively. In general, when the RL < −10 dB, it means that the absorbing material can absorb more than 90% of the incident electromagnetic waves, and when the RL < −20 dB, it means that the absorber will absorb more than 99% of the incident electromagnetic waves [44].

Excellent performance electromagnetic wave absorbing materials are characterized by thin matching thickness, high reflection loss capability, and wide effective absorption bandwidth. From Equations (1) and (2), we can calculate the corresponding material thickness versus reflection loss at 2–18 GHz. It is well known that RLmin value is an important index to evaluate the performance of absorbing materials. Figure 4a–i show the corresponding 3D, 2D and 1D reflection loss plots for all samples in the 2–18 GHz range for frequency and thickness. Comparing the RL values of SiO₂@NiFe LDH at different matching thicknesses, the S3 sample exhibits excellent electromagnetic wave absorption performance at small thicknesses. The best RL values for S1, S2 and S3 samples are −25.18 dB, −31.76 dB and −53.78 dB, respectively; and the widest effective absorption bandwidths are 4 GHz, 4.3 GHz and 8.24 GHz, respectively. For the S3 sample, a reflection loss of −53.78 dB can be achieved at an ultra-thin thickness of 6.95 mm, and an effective absorption bandwidth of 8.24 GHz (9.76–18 GHz) can be achieved at 9.5 mm, which is significantly better than the matching of most SiO₂-based core-shell composites' thickness (Table 1), indicating that it is a promising absorbing material. By adjusting the thickness, the bandwidth of S3 occupies the entire Ku band, which is an extremely excellent performance. The performance gap between S1, S2 and S3 is mainly caused by the difference in lamellar spacing, lamellar thickness and NiFe ratio. The S3 sample has a strong absorption ability and wide effective absorption bandwidth, which is due to that when the NiFe ratio is 3 to 3, the LDH nanosheets have larger interlayer spacing and thicker lamellae, and the increase of the interlayer spacing affects the reflection value. The more frequent scattering is beneficial to the construction of the conductive network and also promotes the polarization loss of the incident electromagnetic wave. The magnetic loss caused by the relatively high Fe content can improve its electromagnetic performance [45]. The basal plane between the NiFe-LDH layers is the active surface, so the size of the interlayer spacing determines the wave absorbing performance, and the small interlayer spacing will restrict the electromagnetic wave from entering the interlayers [46].

In general, the magnetic loss mechanism is caused by eddy current effects, natural resonance and exchange resonance in the gigahertz band. The magnetic loss mechanism is characterized by eddy current, which can be expressed as $\mu'' (\mu')^{-2} f^{-1}$. The calculated results are shown in Figure 5a. The value of the eddy current on SiO₂@NiFe LDH fluctuates from 2 to 10 GHz, indicating the eddy current loss is not the main cause of magnetic loss and is consistent with our previous analysis, which can be caused by natural resonances and switching resonances during magnetic loss. In the range of 10–18 GHz, the change of the value of eddy current loss is very small, indicating that the eddy current loss has a greater effect on the attenuation of electromagnetic waves in this frequency range.

Table 1. Comparison of EMW absorption performance of other SiO₂ or NiFe nanocomposite absorbers.

Materials	Percentage (wt.%)	Absorption Peak (GHz)	Minimum RL (dB)	Effective Absorption Bandwidth (GHz)	Absorber Thickness (mm)	Reference
α-Fe ₂ O ₃ @SiO ₂	-	16.00	−4.30	-	3	[46]
Ni/SiO ₂ nanocomposites	50	12–16	−20.00	4.00	2–4	[47]
graphene@SiO ₂ @NiO nanoflowers	25	11.30	−20.50	5.00	3	[13]
MWCNTs/NiFe nanoparticles	15	8.20	−19.00	1.60	4	[45]
NiFe@NC nanoparticles	40	11.96	−46.89	4.10	2.2	[48]
SiO ₂ @NiFe LDH-3	40	16.50	−53.78	8.24	6.95	This work

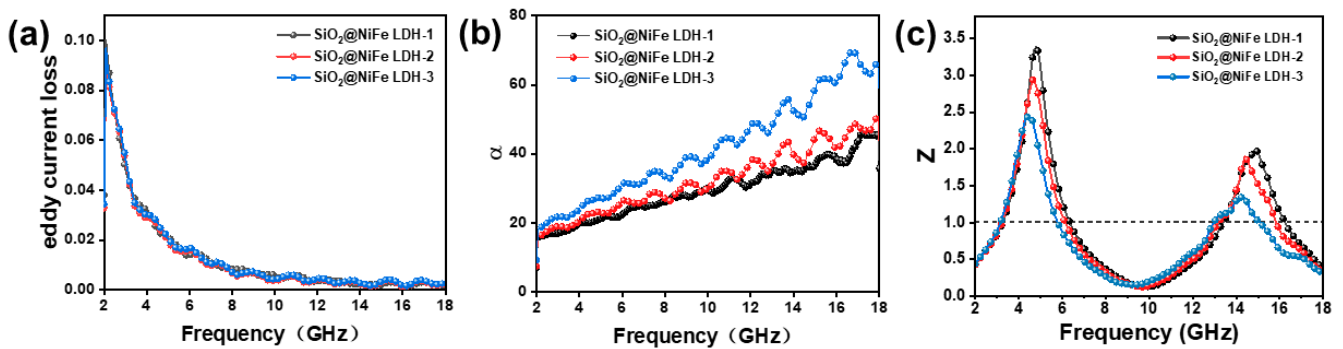


Figure 5. (a) Frequency dependence of eddy current loss, (b) attenuation constant and (c) impedance matching Z_r of the SiO₂@NiFe LDH-1, 2, 3.

The attenuation constant (α) is calculated according to the theoretical formula of the transmission line combined with the measured electromagnetic parameters to reflect the attenuation ability of the absorber [49].

$$\alpha = \left(\sqrt{2}\pi f/c\right) \times \sqrt{(\mu''\epsilon'' - \mu'\epsilon') + \sqrt{(\mu''\epsilon'' - \mu'\epsilon')^2 + (\mu'\epsilon'' + \mu''\epsilon')^2}} \quad (6)$$

$$c_0 = \mu'' (\mu')^{-2} \mu'' (f)^{-1} = 2\pi\mu_0 d^2 \delta \quad (7)$$

where d is the thickness of the absorber and μ is the vacuum permeability. Figure 5b is the correlation curve between the attenuation coefficient and frequency of each sample. With the increase of frequency, the curve changes obviously, but the attenuation system of S3 is more obvious than other samples, which means that S3 has stronger attenuation ability and better absorption performance for incident electromagnetic waves, which is consistent with our previous conclusion.

The impedance-matching characteristic (Z_{in}/Z_o) is another important index to evaluate the electromagnetic wave absorption performance of the wave absorber [50]. For an ideal absorbing material, the reflection value of the incident electromagnetic wave is small or zero is the best. The closer the Z_{in}/Z_o value is to 1, the easier it is for the incident EMW to pass through the absorber layer. The calculated values of Z_{in}/Z_o are shown in Figure 5c. The Z_{in}/Z_o value of the S3 sample is close to 1 and has a smaller fluctuation range. Therefore, the incident electromagnetic wave easily penetrates into the S3 sample and is further attenuated. The optimal impedance matching properties of the S3 sample benefit from the effective tuning of complex permittivity and complex permeability.

Therefore, the functions of each component of the electromagnetic wave absorber are as follows. NiFe LDH, as the main dissipative material, provides excellent conduction losses in core-shell materials. The sheet-like properties of LDH and the SiO₂ spheres as scaffolds are conducive to the free migration of electrons between sheets, forming a conductive pathway, promoting the effect of conductive penetration, and further increasing the conductive loss. The excellent impedance matching due to the excellent lamellar structure can maximize the entry of incident electromagnetic waves, and the nanoflower-like structure can induce multiple scattering to enhance the absorber interaction. At the permeation threshold, SiO₂ microspheres act as connectors, which can significantly improve conduction loss and effectively absorb electromagnetic waves.

The electromagnetic wave absorption mechanism of SiO₂@NiFe LDH is shown in Figure 6. First, NiFe LDH not only has a high specific surface area and abundant inner interface but also has a stable structure, which provides favorable conditions for the maximum attenuation of incident electromagnetic waves inside the absorber in addition to the relatively low electrical conductivity of LDH. It can also provide good impedance matching, which can be obtained by a low dielectric constant, so that more electromagnetic waves can easily enter the material. The electron exchange between ferric ions and divalent nickel ions in NiFe-LDH induces a large number of space charges and polarization charges under the action of alternating electromagnetic fields, both of which increase the dielectric loss capability of the absorber. A large number of heterojunctions between NiFe nanosheets and SiO₂ matrix generate interfacial polarization, which weakens incident electromagnetic waves and leads to dielectric loss. The nano-sized NiFe nanosheet layered structure can act as a dipole to generate a large number of orientation polarizations and transfer the energy of electromagnetic waves converted into heat energy. Finally, the basal plane between the NiFe-LDH layers is the active surface, which is conducive to the construction of the conductive network and also promotes the polarization loss of the incident electromagnetic wave.

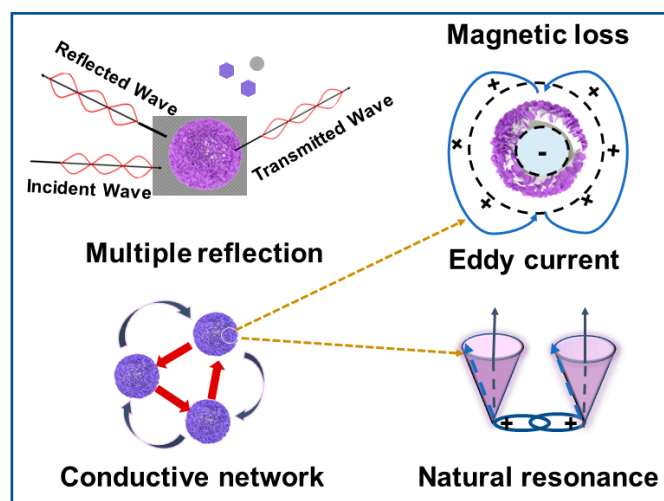


Figure 6. Microwave absorption mechanisms of SiO₂@NiFe LDH.

3. Discussion

In conclusion, NiFe LDH was successfully grown in situ on SiO₂ microspheres by a simple hydrothermal method. The SiO₂@NiFe LDH nanocomposites with different NiFe element ratios prepared in this paper are expected to provide a new method for the design of novel microwave absorbers. The combined effect of excellent magnetic loss and dielectric loss capabilities, good impedance matching, and the effective combination of excellent spherical and lamellar geometry are the mechanisms for its high-efficiency microwave absorption performance. When the mole ratio of Ni and Fe source is 3:3, the SiO₂@NiFe LDH-3 obtained has excellent effective absorption bandwidth (9.76 GHz–18.0 GHz) and the composite has the characteristics of high efficiency, no pollution and low cost. In

addition, it should be emphasized that in the current reports, LDHs are rarely used for electromagnetic wave absorption. It is undoubtedly a meaningful attempt to make use of its unique structure and good physical and chemical characteristics to prepare a new electromagnetic wave absorber.

4. Materials and Methods

4.1. Materials

TEOS (Tetraethyl orthosilicate), C₂H₆O (ethanol), NH₃·H₂O (ammonia), CH₄N₂O (urea), Fe(NO₃)₃·9H₂O (Iron nitrate hexahydrate), Ni(NO₃)₂·6H₂O (Nickel nitrate hexahydrate), C₆H₅O₇Na₃ (trisodium citrate). All chemicals purchased from Aladdin were of analytical purity and used without further purification.

4.2. Synthesis of SiO₂ Microspheres

Using the improved Stöber method, SiO₂ microspheres were prepared by catalyzing hydrolysis and agglomeration with ethyl orthosilicate as the raw material and ethanol as the medium. A quantity of 2 mL TEOS was added dropwise to 50 mL of ethanol with continuous stirring. Subsequently, 5 mL NH₃·H₂O was slowly added to the above solution. Stirring vigorously for 4 h until the clear solution was converted to a white suspension. The white pellet (SiO₂ microspheres) was collected by centrifugation, washed repeatedly three times with deionized water and ethanol, and dried at 70 °C for 12 h.

4.3. Synthesis SiO₂@NiFe LDH Composites

SiO₂@NiFe LDH composites are prepared by a one-step hydrothermal method. Fe(NO₃)₃·9H₂O, Ni(NO₃)₂·6H₂O urea (12 mmol), and trisodium citrate (0.2 mmol) were dispersed into deionized water (65 mL); SiO₂ microspheres (80 mg) prepared in the previous step were added and vigorously stirred for 30 min. Subsequently, the mixed solution is transferred to a Teflon-lined stainless autoclave and sealed to heat at 180 °C for 24 h. After the end of the reaction, the samples were washed alternately with ethanol and water three times and dried in vacuo at 60 °C for 12 h. The total metal ion moles were 1.6 mmol, and three samples were prepared by adjusting the molar ratios of Ni²⁺ and Fe³⁺ to 3:1, 3:2, and 3:3, named SiO₂@NiFe LDH-1,2,3, abbreviated as S1, S2, S3, respectively.

4.4. Material Characterization

The crystallographic information and chemical compositions of the prepared nanostructures were established by powder X-ray diffraction (XRD, D/max 2500, Cu K α), and they were analyzed with the JADE 6.0 software. The magnetic properties were also characterized by a vibrating sample magnetometer (VSM, Lakeshore 7, 304). XPS spectra were acquired on a Physical Electronics ESCA 5600 spectrometer with a monochromatic Al K α X-ray source (power: 200 W/14 kV) and a multichannel detector (Omni IV). Thermogravimetric analysis (TGA, Mettler Toledo TGA/DSC3+, in air at a heating rate of 20 °C/min). In the 2.0–18.0 GHz range with vector network analyzer (VNA; Agilent E5071c) to test the electromagnetic parameters of all samples. The samples were mixed with paraffin (mass ratio 4:6) and pressed into rings with an inner diameter of 3.04 mm, outer diameter of 7.00 mm and thickness of 2 mm. The electromagnetic wave absorption properties of the samples were calculated.

Supplementary Materials: The following supporting information can be downloaded at: <https://www.mdpi.com/article/10.3390/ijms24010504/s1>.

Author Contributions: Z.D. and D.W.: Conceptualization, methodology, investigation, writing—original draft, writing—review and editing; X.Z. and Z.Y.: formal analysis; J.T. and P.Y.: investigation and methodology; R.C.: validation and investigation; S.Y. and J.R.: project administration; Y.Z.: validation, funding acquisition and writing—review and editing. All authors have read and agreed to the published version of the manuscript.

Funding: The authors gratefully acknowledge the financial support provided by Graduate Scientific Research and Innovation Foundation of Chongqing, China (CYS22005, CYB22007), the National Natural Science Foundation of China (Grant No. 52005290, 51908092), Scientific Research Project of Chongqing Ecological Environment Bureau (No. CQEE2022-STHBZZ118), Projects (No. 2020CDJXZ001, 2021CDJMRH-005 and SKLMT-ZZKT-2021M04) supported by the Fundamental Research Funds for the Central Universities, the Joint Funds of the National Natural Science Foundation of China-Guangdong (Grant No. U1801254), the project funded by Chongqing Special Postdoctoral Science Foundation (2021XM3065), the Chongqing Research Program of Basic Research and Frontier Technology (cstc2017jcyjBX0080), Natural Science Foundation Project of Chongqing for Post-doctor (cstc2019jcyjbsH0079, cstc2019jcyjbsHx0085), Technological projects of Chongqing Municipal Education Commission (KJZDK201800801), the Innovative Research Team of Chongqing (CXTDG201602014) and the Innovative technology of New materials and metallurgy (2019CDXYCL0031). The authors also thank the Electron Microscopy Center of Chongqing University for materials characterizations.

Institutional Review Board Statement: Not applicable.

Informed Consent Statement: Not applicable.

Data Availability Statement: The data presented are contained within the article or Supplementary Materials.

Conflicts of Interest: The authors declare no conflict of interest.

References

1. Lin, Z.; Liu, J.; Peng, W.; Zhu, Y.; Zhao, Y.; Jiang, K.; Peng, M.; Tan, Y. Highly Stable 3D Ti₃C₂T_x MXene-Based Foam Architectures toward High-Performance Terahertz Radiation Shielding. *ACS Nano* **2020**, *14*, 2109–2117. [[CrossRef](#)] [[PubMed](#)]
2. Li, J.; Xue, H.; Xu, N.; Zhang, X.; Wang, Y.; He, R.; Huang, H.; Qiao, J. Co/Ni dual-metal embedded in heteroatom doped porous carbon core-shell bifunctional electrocatalyst for rechargeable Zn-air batteries. *Mater. Rep. Energy* **2022**, *2*, 100090. [[CrossRef](#)]
3. Wu, G.; Zhu, W.; He, Q.; Feng, Z.; Huang, T.; Zhang, L.; Schmidt, S.; Godfrey, A.; Huang, X. 2D and 3D orientation mapping in nanostructured metals: A review. *Nano Mater. Sci.* **2020**, *2*, 50–57. [[CrossRef](#)]
4. Jiao, Z.; Huan, W.; Yang, F.; Yao, J.; Tan, R.; Chen, P.; Tao, X.; Yao, Z.; Zhou, J.; Liu, P. Achieving Ultra-Wideband and Elevated Temperature Electromagnetic Wave Absorption via Constructing Lightweight Porous Rigid Structure. *Nano-Micro Lett.* **2022**, *14*, 173. [[CrossRef](#)] [[PubMed](#)]
5. Mohammadabadi, F.H.; Masoudpanah, S.M.; Alamolhoda, S.; Koohdar, H.R. High-performance microwave absorbers based on (CoNiCuZn)(1-x)MnxFe₂O₄ spinel ferrites. *J. Alloys Compd.* **2022**, *909*, 164637. [[CrossRef](#)]
6. Wang, D.; Mukhtar, A.; Humayun, M.; Wu, K.; Du, Z.; Wang, S.; Zhang, Y. A Critical Review on Nanowire-Motors: Design, Mechanism and Applications. *Chem. Rec.* **2022**, *22*, e202200016. [[CrossRef](#)]
7. Zhang, N.; Huang, Y.; Zong, M.; Ding, X.; Li, S.P.; Wang, M.Y. Synthesis of core-shell ZnFe₂O₄@SiO₂ hollow microspheres/reduced graphene oxides for a high-performance EM wave absorber. *Ceram. Int.* **2016**, *42*, 18879–18886. [[CrossRef](#)]
8. Kuang, P.; Ni, Z.; Yu, J.; Low, J. New progress on MXenes-based nanocomposite photocatalysts. *Mater. Rep. Energy* **2022**, *2*, 100081. [[CrossRef](#)]
9. Liu, P.; Yao, Z.; Ng, V.M.H.; Zhou, J.; Kong, L.B.; Yue, K. Facile synthesis of ultrasmall Fe₃O₄ nanoparticles on MXenes for high microwave absorption performance. *Compos. Part A-Appl. Sci. Manuf.* **2018**, *115*, 371–382. [[CrossRef](#)]
10. Wu, Z.; Cheng, H.-W.; Jin, C.; Yang, B.; Xu, C.; Pei, K.; Zhang, H.; Yang, Z.; Che, R. Dimensional Design and Core-Shell Engineering of Nanomaterials for Electromagnetic Wave Absorption. *Adv. Mater.* **2022**, *34*, 2107538. [[CrossRef](#)]
11. Badmus, M.; Liu, J.; Wang, N.; Radacsi, N.; Zhao, Y. Hierarchically electrospun nanofibers and their applications: A review. *Nano Mater. Sci.* **2021**, *2*, 213–232. [[CrossRef](#)]
12. Liu, P.; Yao, Z.; Zhou, J.; Yang, Z.; Kong, L.B. Small magnetic Co-doped NiZn ferrite/graphene nanocomposites and their dual-region microwave absorption performance. *J. Mater. Chem. C* **2016**, *4*, 9738–9749. [[CrossRef](#)]
13. Wang, L.; Huang, Y.; Ding, X.; Liu, P.B.; Zong, M. Ternary nanocomposites of graphene@SiO₂@NiO nanoflowers: Synthesis and their microwave electromagnetic properties. *Micro Nano Lett.* **2013**, *8*, 391–394. [[CrossRef](#)]
14. Qiao, M.T.; Wei, D.; He, X.W.; Lei, X.F.; Wei, J.; Zhang, Q.Y. Novel yolk-shell Fe₃O₄@void@SiO₂@PPy nanochains toward microwave absorption application. *J. Mater. Sci.* **2021**, *56*, 1312–1327. [[CrossRef](#)]
15. Huang, B.; Hu, H.L.; Lim, S.; Tang, X.Z.; Huang, X.Z.; Liu, Y.; Yue, J.L. Gradient FeNi-SiO₂ films on SiC fiber for enhanced microwave absorption performance. *J. Alloys Compd.* **2022**, *897*, 163204. [[CrossRef](#)]
16. Ma, M.; Li, W.; Tong, Z.; Ma, Y.; Bi, Y.; Liao, Z.; Zhou, J.; Wu, G.; Li, M.; Yue, J.; et al. NiCo₂O₄ nanosheets decorated on one-dimensional ZnFe₂O₄@SiO₂@C nanochains with high-performance microwave absorption. *J. Colloid Interface Sci.* **2020**, *578*, 58–68. [[CrossRef](#)]

17. Dai, X.; Yi, W.; Yin, C.; Li, K.; Feng, L.; Zhou, Q.; Yi, Z.; Zhang, X.; Wang, Y.; Yu, Y.; et al. 2D-3D magnetic NiFe layered double hydroxide decorated diatomite as multi-function material for anionic, cationic dyes, arsenate, and arsenite adsorption. *Appl. Clay Sci.* **2022**, *229*, 106664. [[CrossRef](#)]
18. Liu, B.; Zhang, M.; Wang, Y.; Chen, Z.; Yan, K. Facile synthesis of defect-rich ultrathin NiCo-LDHs, NiMn-LDHs and NiCoMn-LDHs nanosheets on Ni foam for enhanced oxygen evolution reaction performance. *J. Alloys Compd.* **2021**, *852*, 156949. [[CrossRef](#)]
19. Zhou, Q.; Dai, X.; Li, K.; Zhang, C.; Zhang, X.; Du, Z.; Yi, S.; Yang, P.; Rao, J.; Zhang, Y. Facile synthesis of a 2D multilayer core-shell MnO₂@LDH@MMT composite with a nanoflower shape for electromagnetic wave absorption. *Crystengcomm* **2022**, *24*, 6546–6557. [[CrossRef](#)]
20. Feng, X.; Jiao, Q.; Chen, W.; Dang, Y.; Dai, Z.; Suib, S.L.; Zhang, J.; Zhao, Y.; Li, H.; Feng, C. Cactus-like NiCo₂S₄@NiFe LDH hollow spheres as an effective oxygen bifunctional electrocatalyst in alkaline solution. *Appl. Catal. B: Environ.* **2021**, *286*, 119869. [[CrossRef](#)]
21. Lu, Y.; Yang, P.G.; Li, Y.H.; Wen, D.D.; Luo, J.S.; Wang, S.H.; Wu, F.; Fang, L.; Pang, Y. A Facile Synthesis of NiFe-Layered Double Hydroxide and Mixed Metal Oxide with Excellent Microwave Absorption Properties. *Molecules* **2021**, *26*, 5046. [[CrossRef](#)] [[PubMed](#)]
22. Guo, Y.; Jian, X.; Zhang, L.; Mu, C.; Yin, L.; Xie, J.; Mahmood, N.; Dou, S.; Che, R.; Deng, L. Plasma-induced FeSiAl@Al₂O₃@SiO₂ core-shell structure for exceptional microwave absorption and anti-oxidation at high temperature. *Chem. Eng. J.* **2020**, *384*, 123371. [[CrossRef](#)]
23. Bhattacharjee, Y.; Bose, S. Core-Shell Nanomaterials for Microwave Absorption and Electromagnetic Interference Shielding: A Review. *ACS Appl. Nano Mater.* **2021**, *4*, 949–972. [[CrossRef](#)]
24. Gu, W.H.; Chen, J.B.; Zhao, Y.; Wang, G.H.; Wang, F.; Zhang, T.Z.; Zhang, B.S. Extending effective microwave absorbing bandwidth of CoNi bimetallic alloy derived from binary hydroxides. *Sci. Rep.* **2020**, *10*, 19196. [[CrossRef](#)]
25. Shen, X.; Yang, S.H.; Yin, P.G.; Li, C.Q.; Ye, J.R.; Wang, G.S. Enhancement in microwave absorption properties by adjusting the sintering conditions and carbon shell thickness of Ni@C submicrospheres. *Crystengcomm* **2022**, *24*, 765–774. [[CrossRef](#)]
26. Li, X.; Feng, J.; Du, Y.; Bai, J.; Fan, H.; Zhang, H.; Peng, Y.; Li, F. One-pot synthesis of CoFe₂O₄/graphene oxide hybrids and their conversion into FeCo/graphene hybrids for lightweight and highly efficient microwave absorber. *J. Mater. Chem. A* **2015**, *3*, 5535–5546. [[CrossRef](#)]
27. Gupta, T.K.; Singh, B.P.; Singh, V.N.; Teotia, S.; Singh, A.P.; Elizabeth, I.; Dhakate, S.R.; Dhawan, S.K.; Mathur, R.B. MnO₂ decorated graphene nanoribbons with superior permittivity and excellent microwave shielding properties. *J. Mater. Chem. A* **2014**, *2*, 4256–4263. [[CrossRef](#)]
28. Li, H.Q.; Hou, Y.H.; Li, L.C. Synthesis of the SiO₂@C composites with high-performance electromagnetic wave absorption. *Powder Technol.* **2019**, *343*, 129–136. [[CrossRef](#)]
29. Jiang, D.B.; Jing, C.; Yuan, Y.; Feng, L.; Liu, X.; Dong, F.; Dong, B.; Zhang, Y.X. 2D-2D growth of NiFe LDH nanoflakes on montmorillonite for cationic and anionic dye adsorption performance. *J. Colloid Interface Sci.* **2019**, *540*, 398–409. [[CrossRef](#)]
30. Li, K.; Hu, Z.; Zhao, R.; Zhou, J.; Jing, C.; Sun, Q.; Rao, J.; Yao, K.; Dong, B.; Liu, X.; et al. A multidimensional rational design of nickel-iron sulfide and carbon nanotubes on diatomite via synergistic modulation strategy for supercapacitors. *J. Colloid Interface Sci.* **2021**, *603*, 799–809. [[CrossRef](#)]
31. Zhang, Y.; Cai, R.; Wang, D.; Li, K.; Sun, Q.; Xiao, Y.; Teng, H.; Huang, X.; Sun, T.; Liu, Z.; et al. Lightweight, Low-Cost Co₂SiO₄@diatomite Core-Shell Composite Material for High-Efficiency Microwave Absorption. *Molecules* **2022**, *27*, 1055. [[CrossRef](#)]
32. Chen, F.; Zhang, S.; Guo, R.; Ma, B.; Xiong, Y.; Luo, H.; Cheng, Y.; Wang, X.; Gong, R. 1D magnetic nitrogen doped carbon-based fibers derived from NiFe Prussian blue analogues embedded polyacrylonitrile via electrospinning with tunable microwave absorption. *Compos. Part B-Eng.* **2021**, *224*, 109161. [[CrossRef](#)]
33. Yu, M.; Liu, P.-R.; Liu, J.-H.; Li, S.-M.; Wang, C.; Sun, Y.-J. Fabrication and Electromagnetic Microwave Absorbing Properties of NiFe₂O₄/T-ZnOw Composites. *Chin. J. Inorg. Chem.* **2011**, *27*, 1743–1747.
34. Yang, X.; Shu, T.; Yang, X.; Qiao, M.; Wang, D.; Li, X.; Rao, J.; Liu, Z.; Zhang, Y.; Yang, P.; et al. MOFs-Derived Three-Phase Microspheres: Morphology Preservation and Electromagnetic Wave Absorption. *Molecules* **2022**, *27*, 4773. [[CrossRef](#)]
35. Cai, R.; Zheng, W.; Yang, P.; Rao, J.; Huang, X.; Wang, D.; Du, Z.; Yao, K.; Zhang, Y. Microstructure, Electromagnetic Properties, and Microwave Absorption Mechanism of SiO₂-MnO-Al₂O₃ Based Manganese Ore Powder for Electromagnetic Protection. *Molecules* **2022**, *27*, 3758. [[CrossRef](#)]
36. Yang, P.-A.; Huang, Y.; Li, R.; Huang, X.; Ruan, H.; Shou, M.; Li, W.; Zhang, Y.; Li, N.; Dong, L. Optimization of Fe@Ag core-shell nanowires with improved impedance matching and microwave absorption properties. *Chem. Eng. J.* **2022**, *430*, 132878. [[CrossRef](#)]
37. Jia, H.; Yang, X.; Kong, Q.-Q.; Xie, L.-J.; Guo, Q.-G.; Song, G.; Liang, L.-L.; Chen, J.-P.; Li, Y.; Chen, C.-M. Free-standing, anti-corrosion, super flexible graphene oxide/silver nanowire thin films for ultra-wideband electromagnetic interference shielding. *J. Mater. Chem. A* **2021**, *9*, 1180–1191. [[CrossRef](#)]
38. Wang, Q.; Wang, J.; Zhao, Y.; Zhao, Y.; Yan, J.; Deng, Z.; Zhang, H.; Zhao, W.; Tian, J.; Yun, J.; et al. NiO/NiFe₂O₄@N-doped reduced graphene oxide aerogel towards the wideband electromagnetic wave absorption: Experimental and theoretical study. *Chem. Eng. J.* **2022**, *430*, 132814. [[CrossRef](#)]
39. Gu, X.; Zhu, W.; Jia, C.; Zhao, R.; Schmidt, W.; Wan, Y. Synthesis and microwave absorbing properties of highly ordered mesoporous crystalline NiFe₂O₄. *Chem. Commun.* **2011**, *47*, 5337–5339. [[CrossRef](#)]

40. Lu, Z.; Wang, Y.; Di, X.; Wang, N.; Cheng, R.; Yang, L. Heterostructure design of carbon fiber@graphene@layered double hydroxides synergistic microstructure for lightweight and flexible microwave absorption. *Carbon* **2022**, *197*, 466–475. [[CrossRef](#)]
41. Qiu, X.; Wang, W. Removal of borate by layered double hydroxides prepared through microwave-hydrothermal method. *J. Water Process Eng.* **2017**, *17*, 271–276. [[CrossRef](#)]
42. Wu, H.; Zhao, Z.; Wu, G. Facile synthesis of FeCo layered double oxide/raspberry-like carbon microspheres with hierarchical structure for electromagnetic wave absorption. *J. Colloid Interface Sci.* **2020**, *566*, 21–32. [[CrossRef](#)] [[PubMed](#)]
43. Zhao, X.; Nie, X.; Li, Y.; Pu, Y.; Sun, X.; Yu, R.; Liu, X.; Shui, J. A layered double hydroxide-derived exchange spring magnet array grown on graphene and its application as an ultrathin electromagnetic wave absorbing material. *J. Mater. Chem. C* **2019**, *7*, 12270–12277. [[CrossRef](#)]
44. Luo, H.; Ma, B.; Chen, F.; Zhang, S.; Xiong, Y.; Cheng, Y.; Gong, R. Bimetallic Oxalate Rod-Derived NiFe/Fe₃O₄@C Composites with Tunable Magneto-dielectric Properties for High-Performance Microwave Absorption. *J. Phys. Chem. C* **2021**, *125*, 24540–24549. [[CrossRef](#)]
45. Naidu, M.K.; Ramji, K.; Santhosi, B.V.S.R.N.; Murthy, K.K.; Subrahmanyam, C.; Satyanarayana, B. Influence of NiFe Alloy Nanopowder on Electromagnetic and Microwave Absorption Properties of MWCNT/Epoxy Composite. *Adv. Polym. Technol.* **2018**, *37*, 622–628. [[CrossRef](#)]
46. Fu, H.H.; Guo, Y.; Yu, J.; Shen, Z.; Zhao, J.; Xie, Y.; Ling, Y.; Ouyang, S.; Li, S.Q.; Zhang, W. Tuning the shell thickness of core-shell alpha-Fe₂O₃@SiO₂ nanoparticles to promote microwave absorption. *Chin. Chem. Lett.* **2022**, *33*, 957–962. [[CrossRef](#)]
47. Gong, C.; Wang, X.; Zhang, X.; Zhao, X.; Meng, H.; Jia, Y.; Zhang, J.; Zhang, Z. Synthesis of Ni/SiO₂ nanocomposites for tunable electromagnetic absorption. *Mater. Lett.* **2014**, *121*, 81–84. [[CrossRef](#)]
48. Qu, X.H.; Zhou, Y.L.; Li, X.Y.; Javid, M.; Huang, F.R.; Zhang, X.F.; Dong, X.L.; Zhang, Z.D. Nitrogen-doped graphene layer-encapsulated NiFe bimetallic nanoparticles synthesized by an arc discharge method for a highly efficient microwave absorber. *Inorg. Chem. Front.* **2020**, *7*, 1148–1160. [[CrossRef](#)]
49. Park, K.-Y.; Han, J.-H.; Lee, S.-B.; Kim, J.-B.; Yi, J.-W.; Lee, S.-K. Fabrication and electromagnetic characteristics of microwave absorbers containing carbon nanofibers and NiFe particles. *Compos. Sci. Technol.* **2009**, *69*, 1271–1278. [[CrossRef](#)]
50. Wei, Z.; Yang, S.; Jiao, P.; Li, J.; Lu, H.; Li, Y.; He, X.; Yuan, Y. Novel and effective strategy for producing NiFe alloy fibers with tunable microwave absorption performance. *Materialia* **2019**, *8*, 100495. [[CrossRef](#)]

Disclaimer/Publisher’s Note: The statements, opinions and data contained in all publications are solely those of the individual author(s) and contributor(s) and not of MDPI and/or the editor(s). MDPI and/or the editor(s) disclaim responsibility for any injury to people or property resulting from any ideas, methods, instructions or products referred to in the content.